Electronic Supplementary Material (ESI) for Chemical Communications.

Bioinspired Photoelectrochemical NADH Regeneration Based on a Molecular-Modified Photocathode

Meng Chen,[†a,b] Fengyu Liu,[†b] Yizhou Wu,[c] Yingzheng Li,[a] Chang Liu,[a] Ziqi Zhao,[a] Peili Zhang,[a] Yilong Zhao,[a,c] Licheng Sun[a,c] and Fusheng Li[a*]

a) State Key Laboratory of Fine Chemicals, Frontier Science Center for Smart Materials, Dalian University of Technology, 116024 Dalian, China. E-mail: fusheng@dlut.edu.cn

b) Department of Chemistry, Dalian University of Technology, 116024 Dalian, China

c) Center of Artificial Photosynthesis for Solar Fuels and Department of Chemistry, School of Science and Research Center for Industries of the Future, Westlake University, 310024 Hangzhou, China

† These authors contributed equally to this work.

Experimental Section

Materials and Reagents

Dibasic Sodium Phosphate (Na_2HPO_4, 99%), Sodium Dihydrogen Phosphate (NaH_2PO_4, 99.5%), Sodium hydroxide (NaOH, 99%), 4,4'-dioctyl-2,2'-bipyridine ($C_{26}H_{40}N_2$, 98%), Bis[(pentamethylcyclopentadienyl)-dichloro-rhodium] ($[Rh(Cp^*)Cl_2]_2$, 99.99%), potassium hexafluorophosphate (KPF_6, 99%), Gallium Indium eutectic (Ga-In, 99.99%), 4,4'-(1,4-phenylene)bis(1-octylpyridin-1-ium) ($C_{16}H_{12}N_2$, 99%), 1-Bromooctane (C_8H_{18}, 99%) were purchased from Aladdin®. Single polished p-type silicon (P doped, 1-5 Ω cm, thickness 500 μm, <100>) purchased from Suzhou Crystal Silicon Electronic & Technology. The high-purity water (18.2 MΩ·cm^{-1}) used in all tests was supplied by a Milli-Q system. All other reagents were commercially available and used as received. All organic solvents were provided from local suppliers with no further purification.

Physical Characterization Instruments

The surface morphology of electrodes was characterized by JEOL JSM-7900F field emission scanning electron microscope (FE-SEM, 5 kV), the corresponding energy dispersive X-ray (EDX) was obtained by Oxford EDS Inca Energy Coater 300 (15 kV). The samples for STEM were obtained by focus ion beam slicing (ZEISS Crossbeam 540). The surface composition

of the photoanodes was investigated by X-ray photoelectron spectroscopy (XPS) on an ESCALAB Xi+ (Thermo Scientific). The catalyst loading amount of catalyst was obtained by inductively coupled plasma-atomic emission spectroscopy (ICP-AES, AVIO 500 PerkinElmer™). The pH of the electrolyte was measured by the 914 pH/conductometer (Metrohm™). NMR spectra were recorded on a Bruker Advance 500 spectrometer, Bruker Avance II 400 spectrometer and Bruker Avance NEO 600M NMR Spectroscopy. Mass spectrometry measurements were performed on a Bruker MALDI-TOF spectrometer.

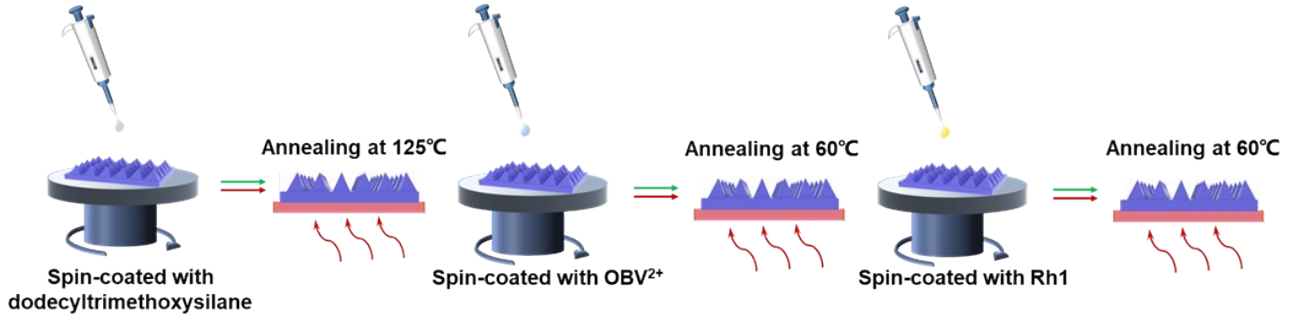

Figure S1. Schematic diagram of the preparation process for electrode-supported "lipid bilayer membrane" photocathodes.

Synthesis

The monomer of OBV^{2+} was synthesized as shown in Scheme S1 , in detail, 4,4'-(1,4-phenylene) bis (1-octylpyridin-1-ium) (500mg), N, N-Dimethylformamide (DMF, 50 mL) and excess 1-Bromooctane ($C_8H_{17}Br$, ~10 equivalent) were added into a flask. The mixture was refluxed at 110 °C for 10 h. After the reaction cooled to room temperature, the precipitate was collected, and washed by Et_2O to remove the unreacted $C_8H_{17}Br$. Pure $OBV^{2+} \cdot 2Br^-$ could be obtained. Finally, $OBV^{2+} \cdot 2Br^-$ was dissolved in H_2O (100 mL), and excess KPF_6 solid was added. $OBV^{2+} \cdot 2PF_6^-$ (named OBV^{2+}) was precipitated and collected, which was washed by MeOH and Et_2O several times. ^1H NMR (600 MHz, CD_2Cl_2) δ = 8.70 (d, *J*=6.4, 4H), 8.29 (d, *J*=6.3, 4H), 7.98 (s, 4H), 4.58 (t, *J*=7.6, 4H), 2.11 – 2.03 (m, 4H), 1.45 – 1.36 (m, 8H), 1.34 – 1.25 (m, 12H), 0.89 (t, *J*=7.0, 6H). ^{13}C NMR (500 MHz, Dichloromethane-D2): 157.93, 154.33, 151.06, 128.74, 123.79, 97.28, 35.84, 32.21, 30.49, 29.69, 23.02, 14.21, 9.12. MS (ESI, m/z): calcd. for 603.33 $[C_{32}H_{46}N_2\text{-}PF6^-]^+$, found m/z^+= 603.28.

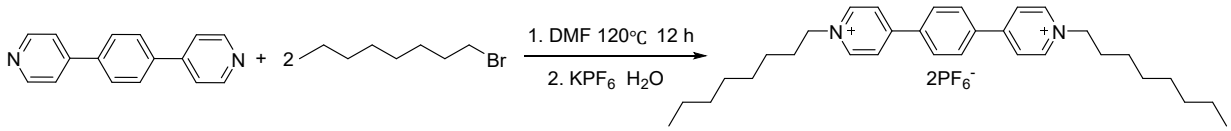

Scheme S1. Synthetic routes of OBV^{2+}.

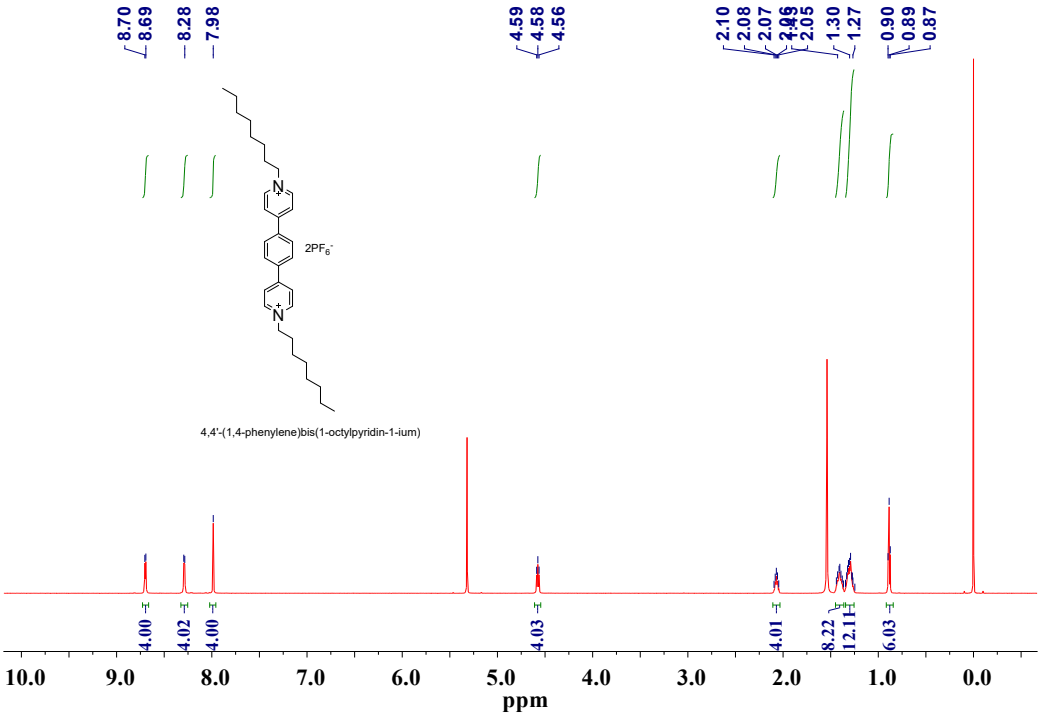

Figure S2. ^{1}H-NMR spectrum of OBV^{2+}.

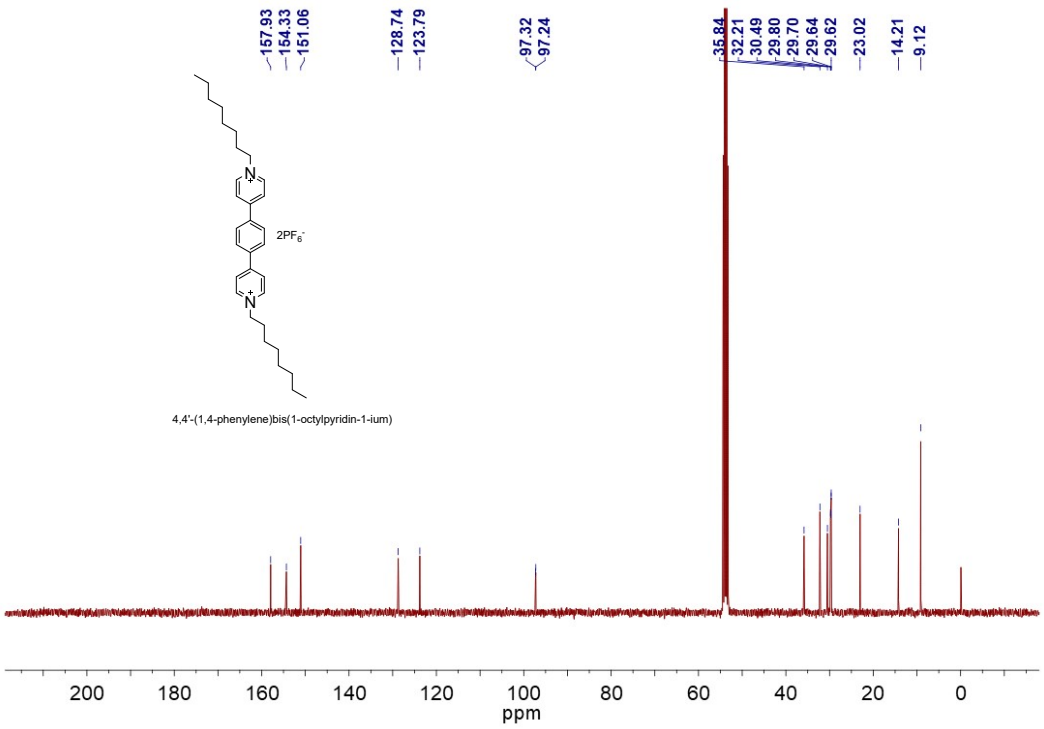

Figure S3. ^{13}C-NMR spectrum of OBV^{2+}.

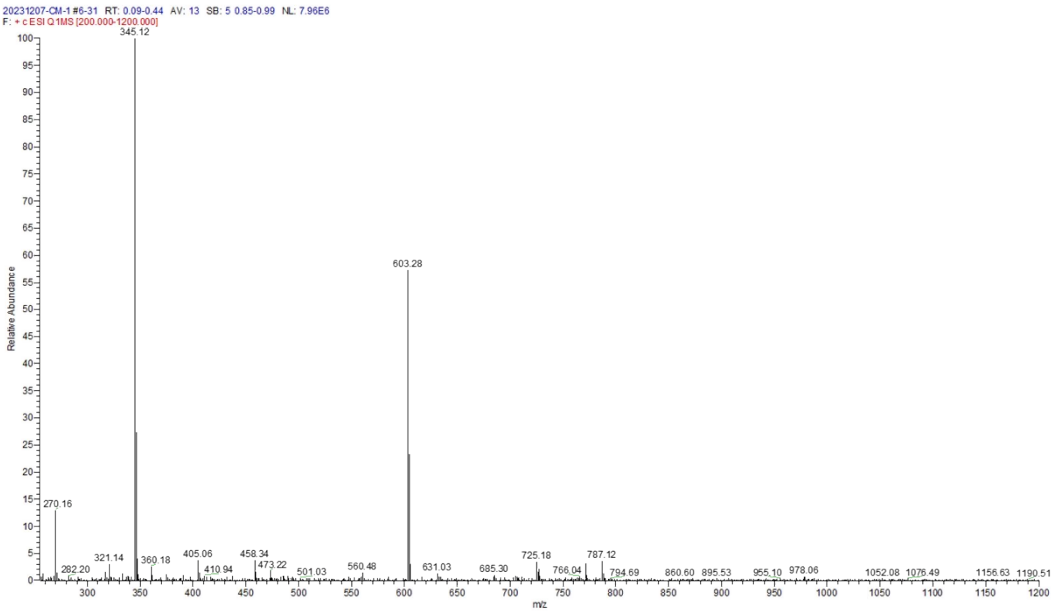

Figure S4. Mass spectrum of OBV^{2+}.

Rh1 was synthesized, as shown in Scheme S2. 4,4'- nonyl -2,2'-bipyridine (403 mg) was mixed with $(RhCp^*Cl_2)_2$ (311 mg) in CH_3OH (10 mL) and was stirred for 4 hours. After evaporating CH_3OH, 15 mL of ether was added and stirred overnight. After filtration of ether, the product was obtained in quantitative yield. Finally, the product was dissolved in H_2O (30

mL), and excess KPF_6 solid was added. The Rh1 molecule is finally obtained after extraction and filtration. ^{1}H NMR (400 MHz, MeOD) δ 8.82 (d, *J* = 5.6, 2H), 8.47 (s, 2H), 7.70 (d, *J* = 5.7, 2H), 2.90 (t, *J* = 7.7, 4H), 1.83 – 1.74 (m, 4H), 1.72 (s, 15H), 1.35 (m, 24H), 0.89 (t, *J* = 5.9, 6H). ^{13}C NMR (500 MHz, Dichloromethane-D2): 155.89, 155.30, 152.04, 129.70, 124.76, 98.28, 98.22, 36.79, 33.17, 30.59, 23.98, 15.18, 10.07, HRMS (ESI, m/z): calcd. for 681.3418 $[C_{38}H_{59}ClN_2Rh]+$, found m/z+= 681.3420

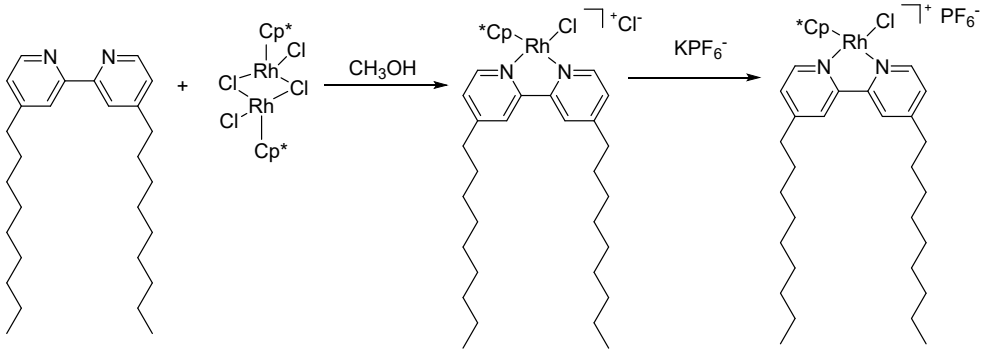

Scheme S2. Synthetic routes of Rh1.

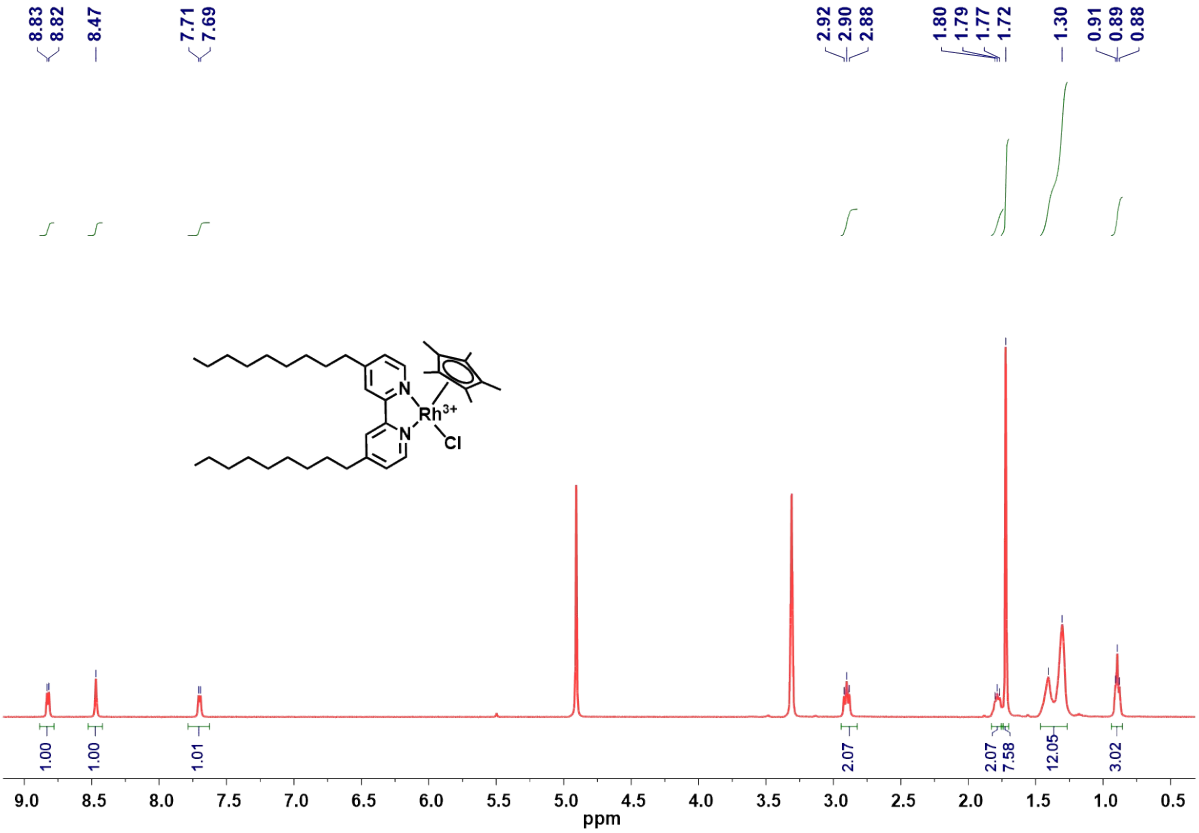

Figure S5. ^{1}H-NMR spectrum of Rh1.

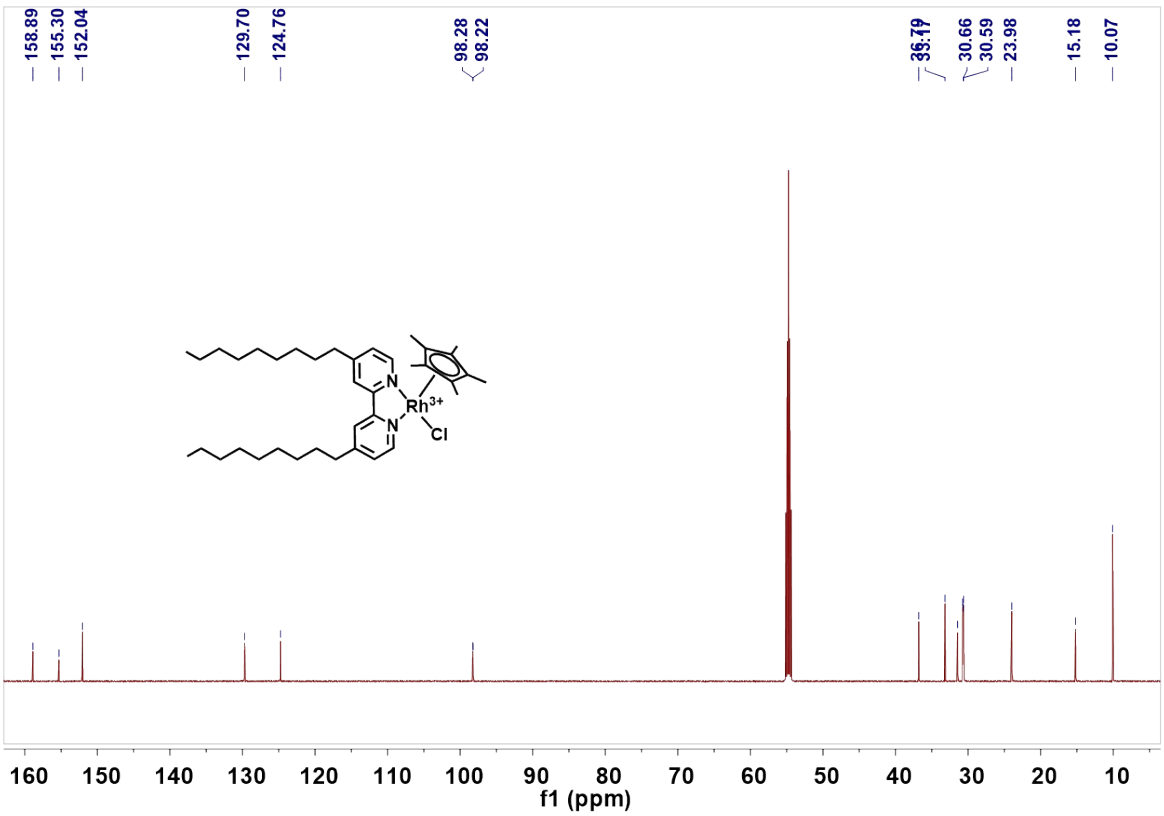

Figure S6. ^{13}C-NMR spectrum of Rh1.

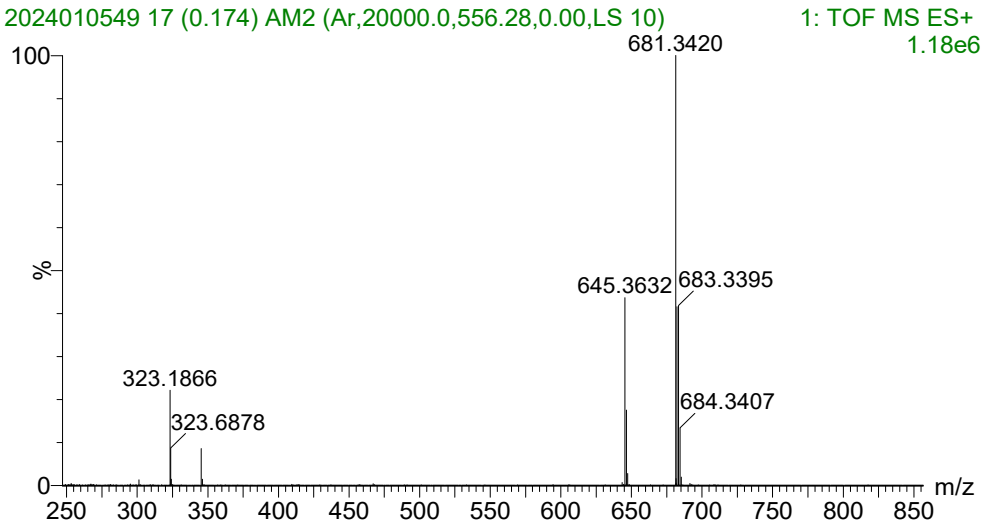

Figure S7. High-resolution mass spectrum of Rh1.

Pretreatment of the Silicon Wafers. The p-type silicon wafer was cut into 1 × 1cm chips. Before the etching process, the p-type (100) Si (0-5 Ω cm) first were washed ultrasonically with alcohol for 10 min each. After, the p-type silicon substrates were further cleaned by a solution of H_2SO_4/H_2O_2 (3:1) at 90 °C for 30 min. The p-type silicon substrates

were immersed in a 5% HF aqueous solution for 5 min to remove the oxide layer on the surface. After cleaned with ethanol, the substrates were transferred into an aqueous solution of 1.5 wt% NaOH, 1.5 wt% Na_2SiO_3, and 5 vol% isopropanol at 85 °C for 30 min. The ohmic contact of p-Si was formed by rubbing eutectic Ga−In alloy at the backside of the micro-pyramid silicon (p-Si). Then, a copper chip was attached on the surface of the eutectic Ga−In alloy by a silver-conductive paint (SPI, 99%). Finally, the edges and backside of silicon wafers were enclosed by epoxy resin (LOCTITE EA 9462 Henkel).

PEC Measurements. The PEC performance of as-fabricated photoelectrodes were measured in an aqueous solution containing 0.1 M PBS buffer and 1 mM NAD^+ with an electrochemical workstation (CHI760). A standard three-electrode system was used with the prepared samples, a saturated Ag/AgCl electrode and a Pt mesh as working, reference and counter electrodes, respectively. The LSV and I-t curves were recorded under simulated sunlight (AM1.5G, 100 mW cm^{-2}) provided by a solar simulator (Newport). The measured potential versus Ag/AgCl was converted to RHE potential by the Nernst equation:

$$E_{RHE} = E_{Ag/AgCl} + 0.059pH + E_{Ag/AgCl}^{\circ}$$

E_{RHE} and $E_{Ag/AgCl}$ are the potential versus the RHE and measured potential versus Ag/AgCl, respectively, and the value of $E^{\circ}_{Ag/AgCl}$ is 0.1976 V at 25 °C.

The Incident Monochromatic Photon-Electron Conversion Efficiency (IPCE) of the electrodes was measured directly with the Zahner photoelectrochemistry workstation (CIMPS2). The scanning range of the wavelength was from 365 to 1020 nm.

PEC NADH Regeneration. In this experiment, H-type cells were used to determine the yield of NADH. Typically, the reaction solution was composed of 0.5 mM NAD^+ and 100 mM phosphate buffer (pH = 7). A photocathode prepared in accordance with the above steps was used as a working electrode to test the variation of NADH yield over time. At the same time, the effects of assembling OBV^{2+} on NADH regeneration were compared. The concentration of NADH in the solution was monitored via UV−vis characterization.

IMPS Intensity Modulated Photocurrent Spectroscopy (IMPS) Measurements. IMPS spectra were recorded by a Zahner photoelectrochemical workstation (CIMPS-2) for Rh1/SCA/p-Si and Rh1/OBV^{2+}/SCA/p-Si. 10% superimposition of sinusoidal modulation was added onto a white light-emitting diode with an intensity of 100 mW cm^{-2} to obtain the

intensity-modulated light. The modulation amplitude voltage of light-emitting diode was 10 mV. IMPS data was recorded over the 200 kHz to 0.5 Hz frequency range at different applied potentials in 100 mM PBS buffer and 1 mM NAD^+ (pH=7).

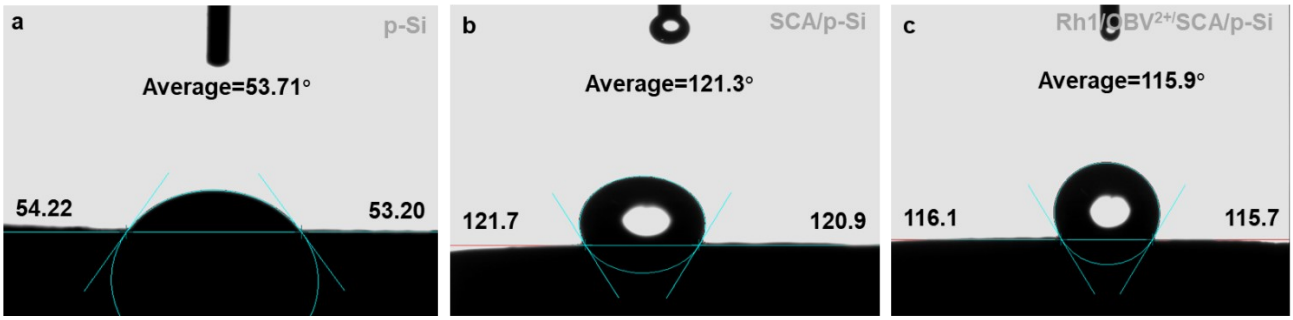

Figure S8. Contact angle measurement of p-Si, SCA/p-Si and Rh1/OBV^{2+}/SCA/p-Si.

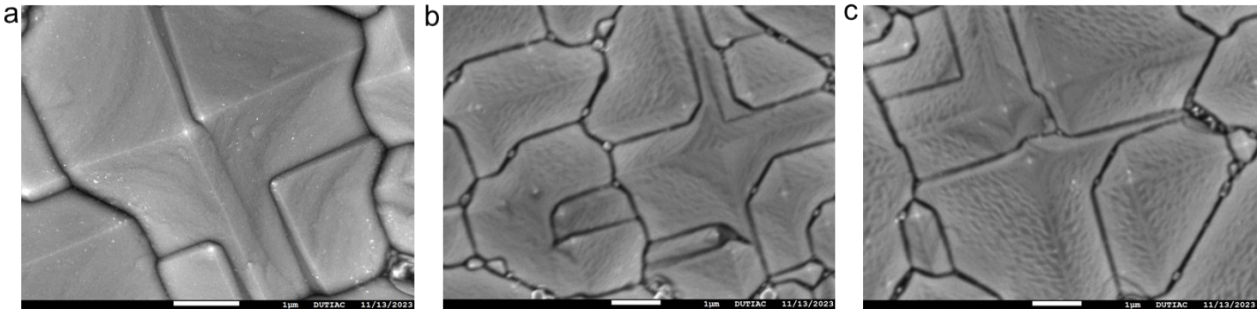

Figure S9. FE-SEM images (a) p-Si; (b) Rh1/SCA/p-Si; (c) Rh1/OBV^{2+}/SCA/p-Si.

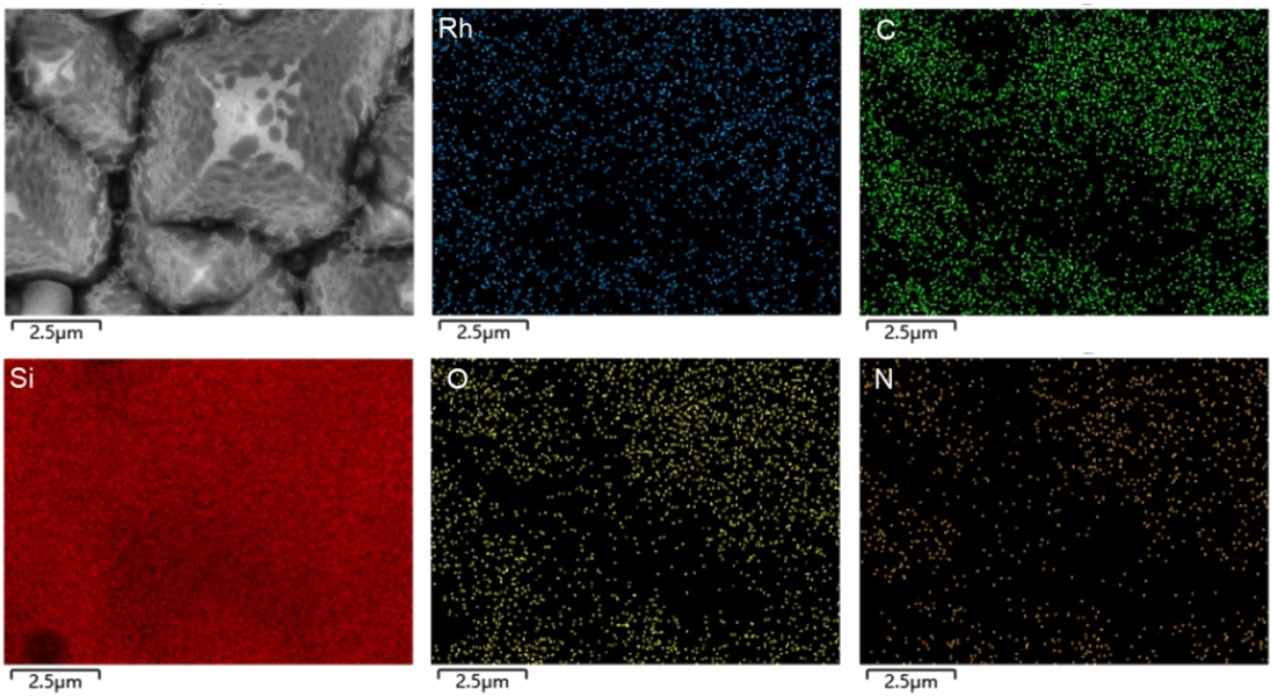

Figure S10. SEM image and EDS elemental mapping of the Rh1/OBV^{2+}/SCA/p-Si film. Elements detected: Si, N, Rh, O, C.

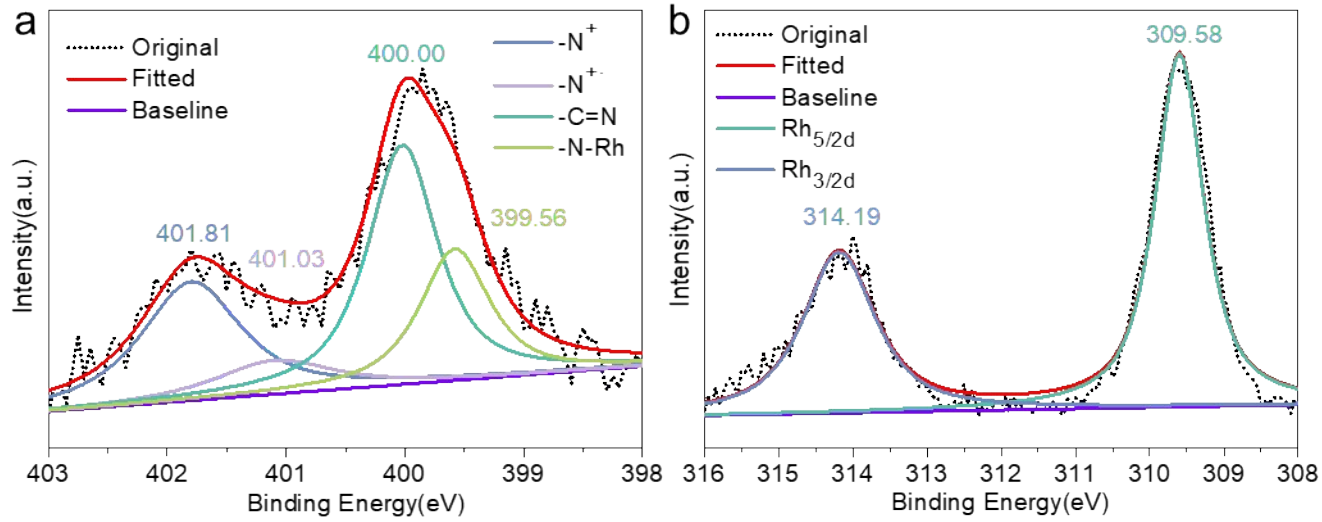

Figure *S11.* XPS spectra of Rh1/OBV^{2+}/SCA/p-Si: (a) N 1s; (b) Rh 3d.

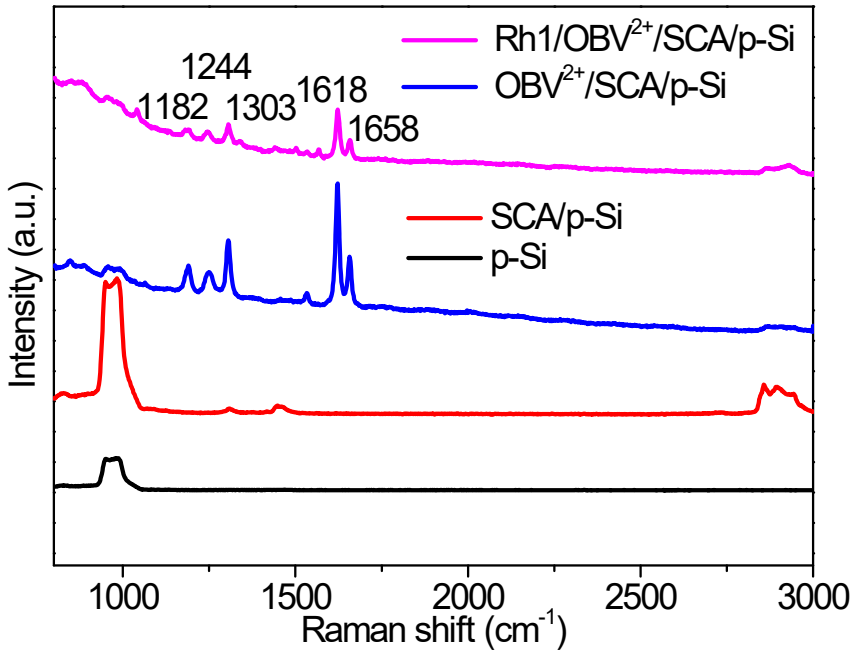

Figure. *S12*. Raman spectrum of photocathodes.

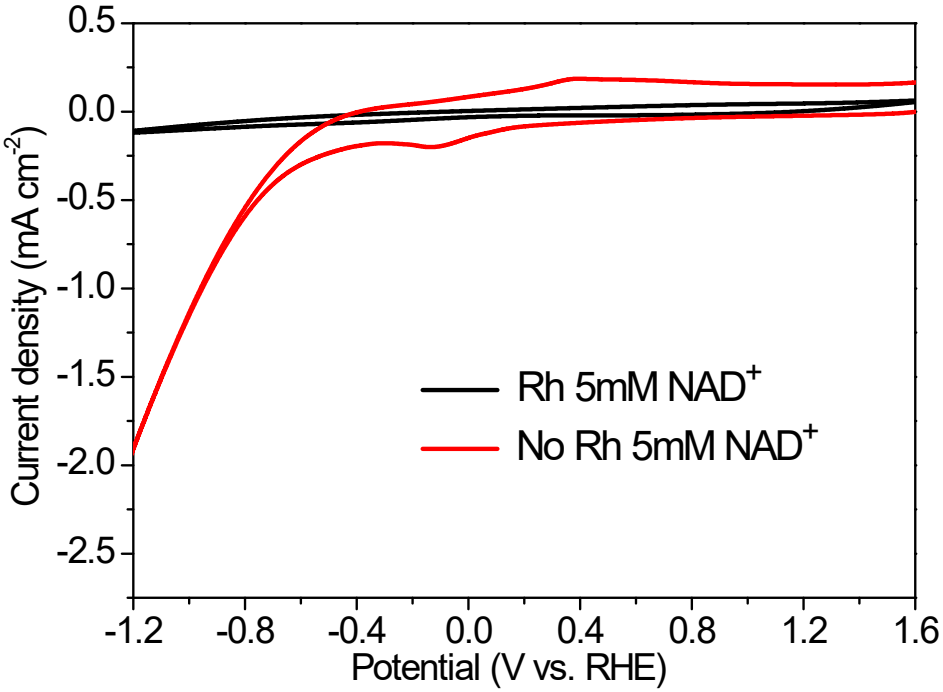

Figure. *S13*. Cyclic voltammograms of 5 mM NAD^+ with and without Rh1 recorded using a glassy carbon electrode, in 100 mM PBS buffer (pH 7) under nitrogen with a scan rate of 100 mV s^{-1}.

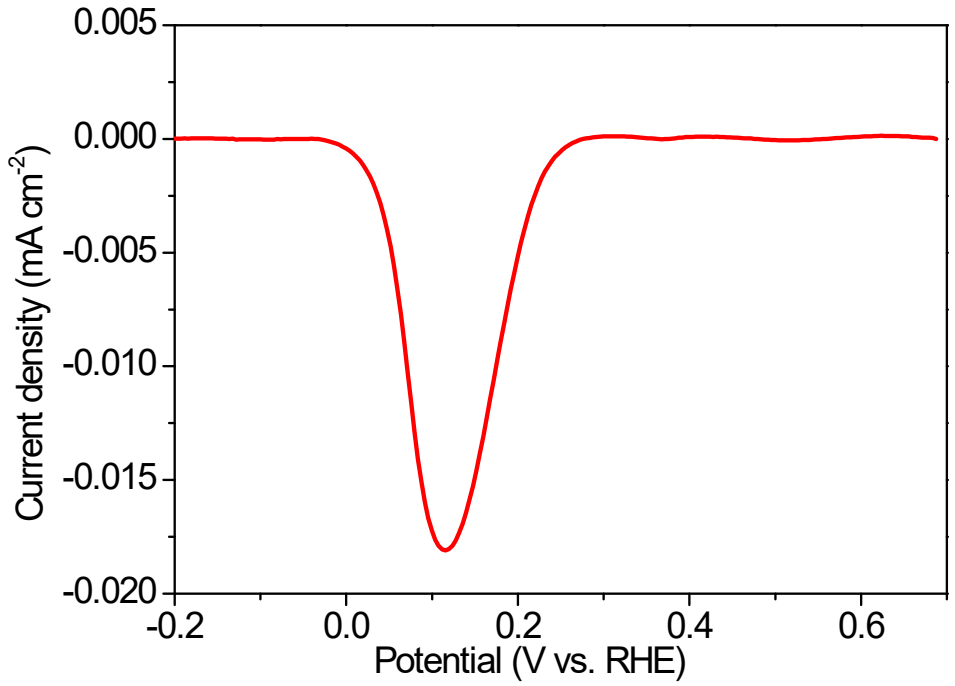

Figure. *S14*. Differential pulse voltammogram (DPV) of Rh1 recorded using a glassy carbon electrode in 100 mM PBS buffer (pH 7) under nitrogen with a scan rate of 100 mV s^{-1}.

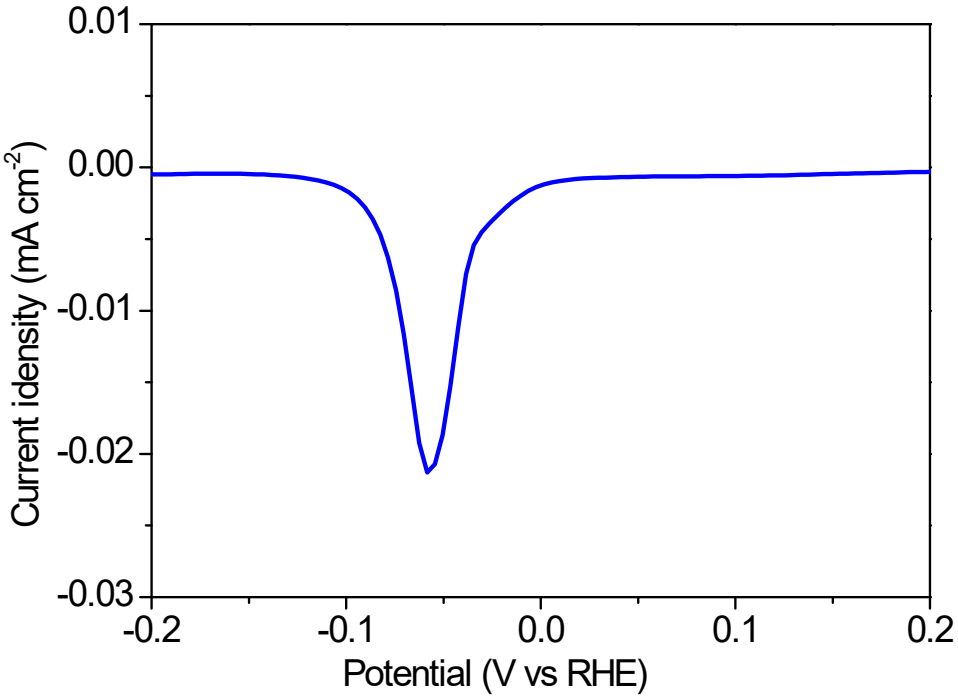

Figure *S15.* DPV of OBV^{2+} recorded using a glassy carbon electrode in 100 mM PBS buffer (pH 7) under nitrogen with a scan rate of 100 mV s^{-1}.

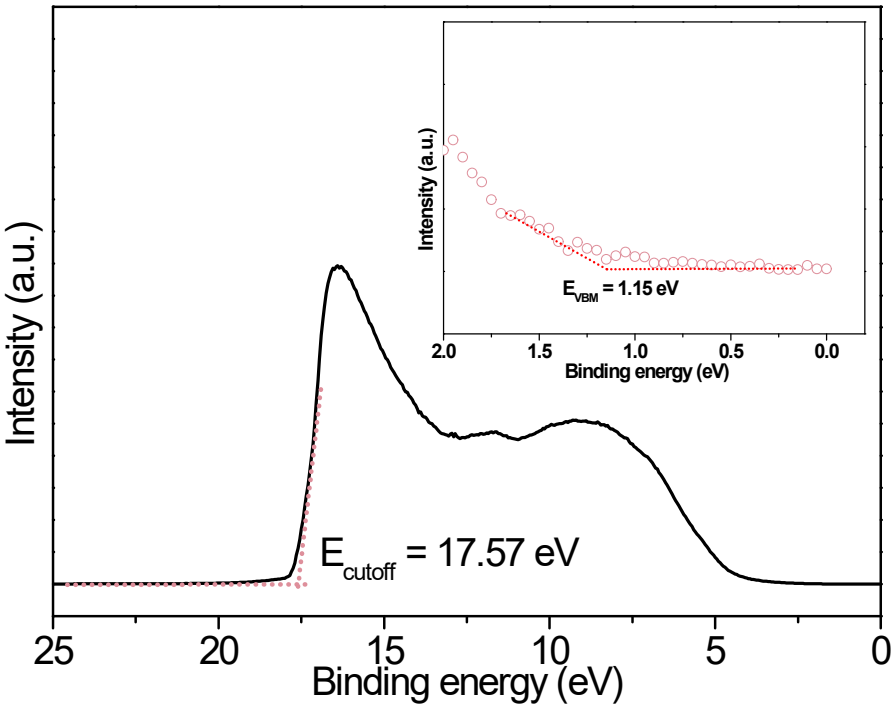

Figure *S16.* UPS spectra of the p-Si for valence band (VB) determination. The insert shows the enlarged VB position of p-Si.

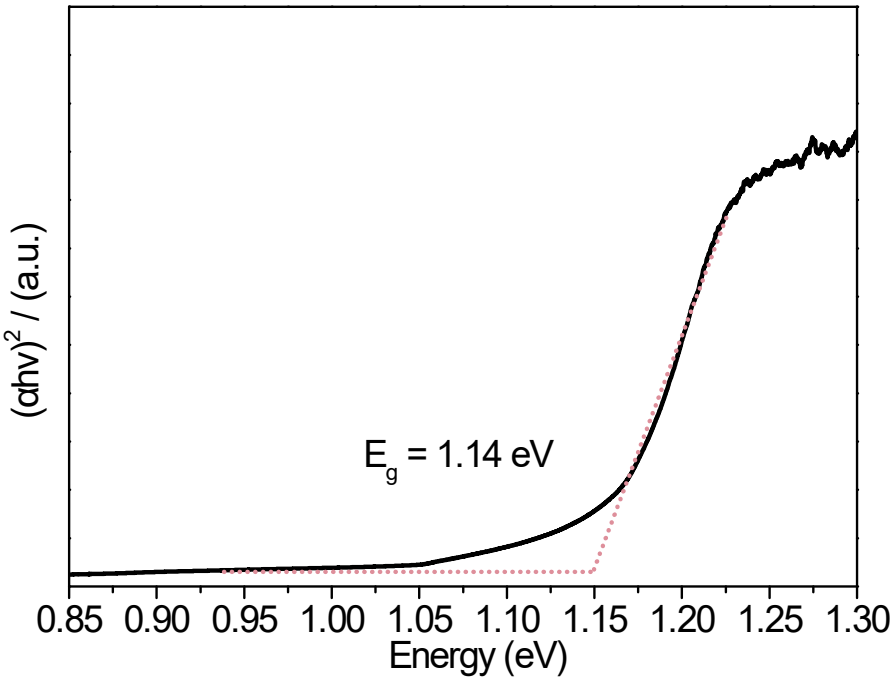

Figure *S17.* Tauc plot of p-Si calculated by using UV-vis absorbance spectrum.

The work function (E_{work} corresponding to the Fermi level), VB, and conduction band (CB) of p-Si were determined according to the following equations.

$$E_{Work} = h\nu - (E_{cutoff} - E_F) = 21.2 - 17.57 = 3.63 \text{ eV} \quad \text{Eq. S1}$$

$$E_{VB} = E_{work} + E_{VBM} = 3.63 + 1.16 = 4.79 \text{ eV} \quad \text{Eq. S2}$$

$$E_{CB} = E_{VB} - E_g = 4.79 - 1.14 = 3.65 \text{ eV} \quad \text{Eq. S3}$$

Where, the E_{cutoff} is the cut-off energy edge, the E_F is initial edge energy, the E_{VBM} is the energy from valence band maximum to Fermi level, the E_g is bandgap energy (obtained by UV-vis spectra), the E_{VB} is valance band energy and the E_{CB} is conduction band energy.

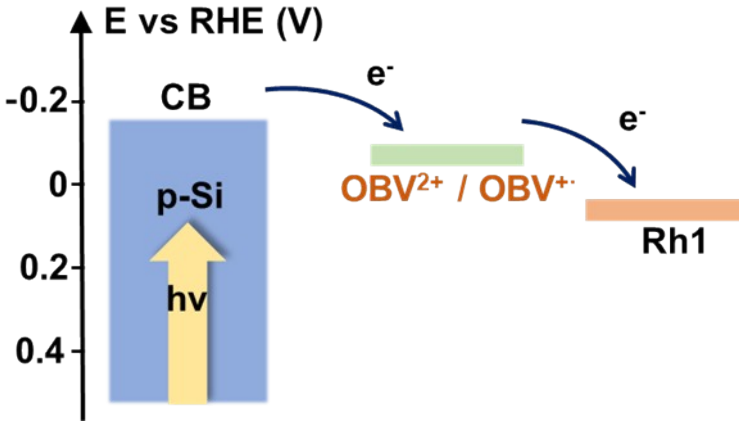

Figure S18. The electron energy profile of the ECB for p-Si; the redox potential of OBV2+ and Rh1.

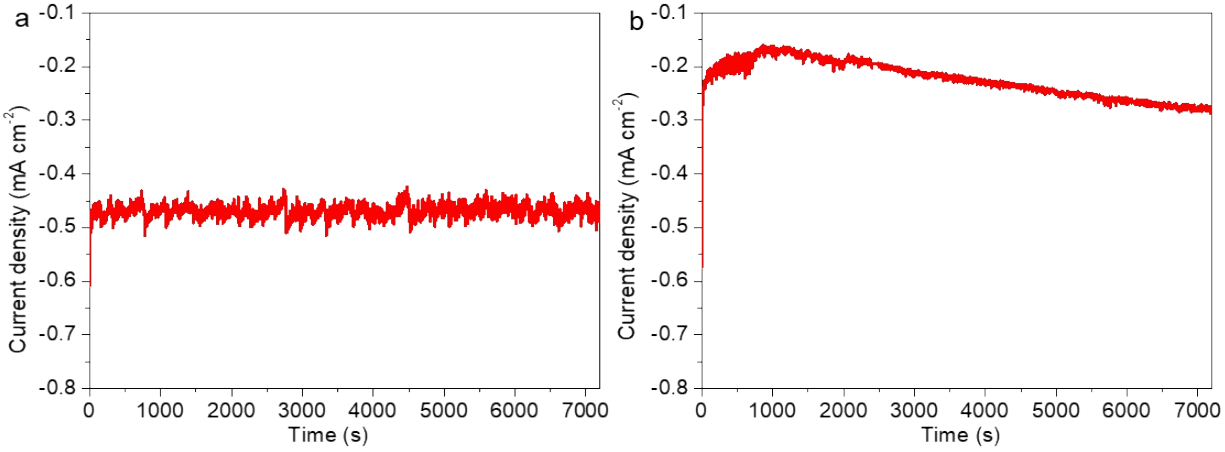

Figure S19. *I-t* curves of (a) Rh1/OBV^{2+}/SCA/p-Si electrode and (b) Rh1/SCA/p-Si electrode in 0.5 mM of NAD$^+$ and 0.1 M PBS (pH = 7, 10 mL) at an applied potential of −0.6 V vs. RHE for 2 h.

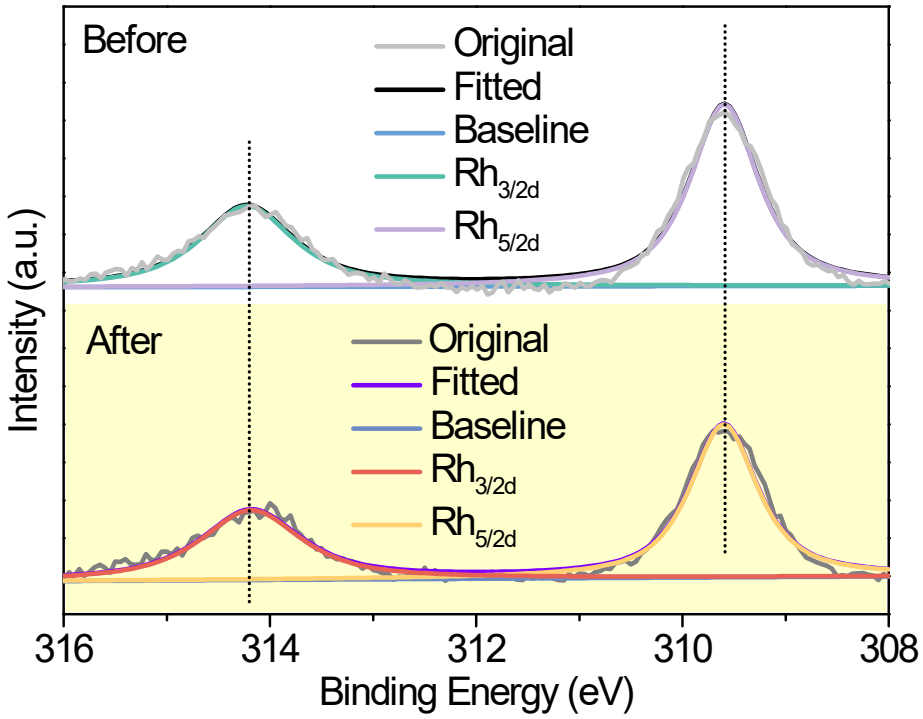

Figure S20. XPS spectra of the Rh 3d signal before and after regeneration of NADH for the Rh1/OBV^{2+}/SCA/p-Si electrode.

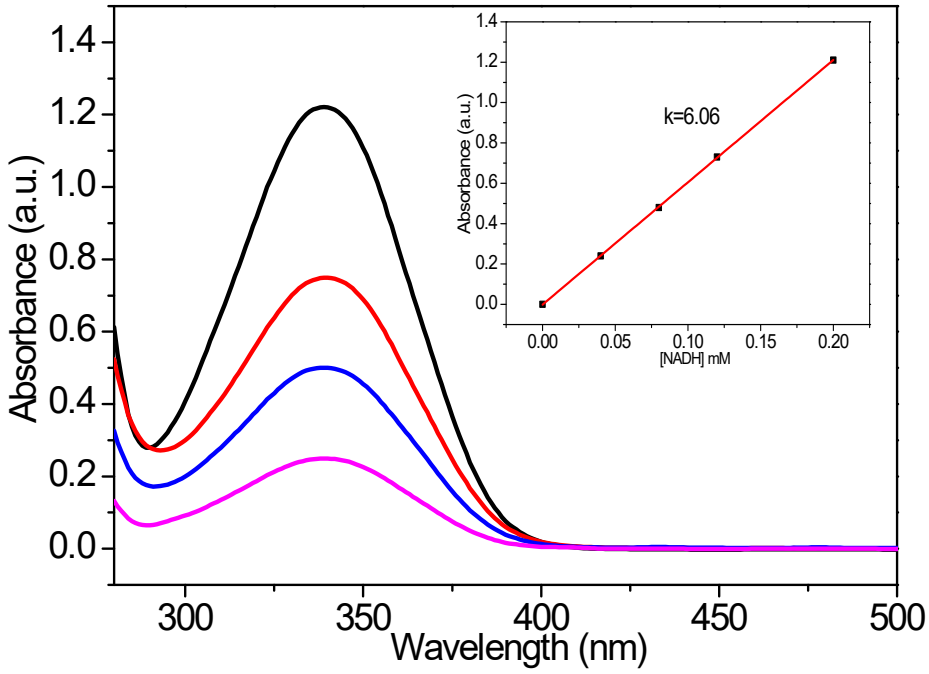

Figure S21. UV–vis absorption spectra of commercial 1,4-NADH. The insert shows calibration curve between A340 and the concentration of 1,4-NADH.

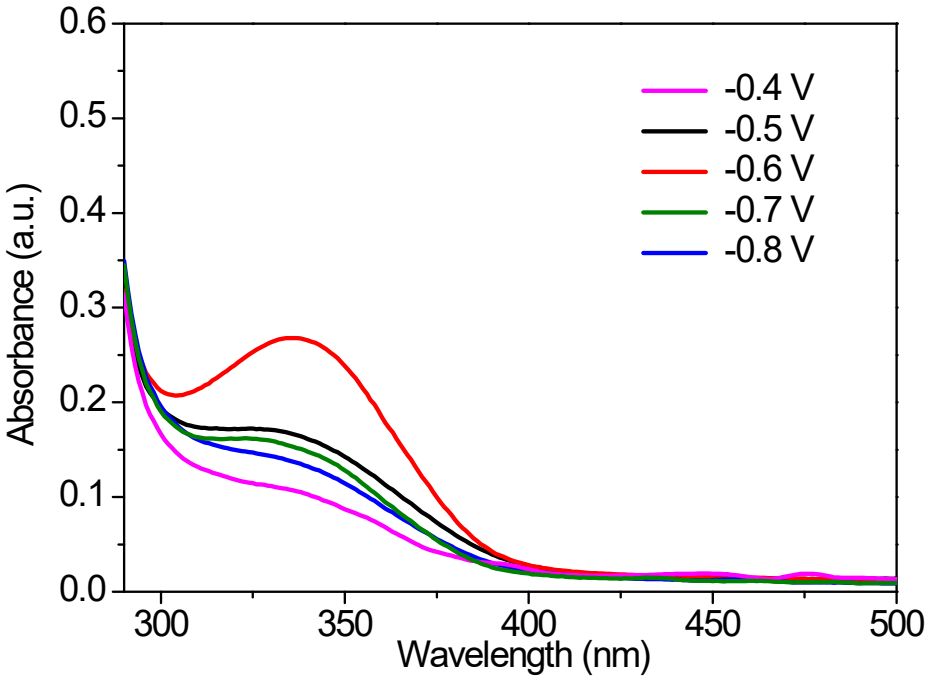

Figure *S22.* UV−vis spectra of the NDAH regeneration using Rh1/OBV^{2+}/SCA/p-Si at different potentials.

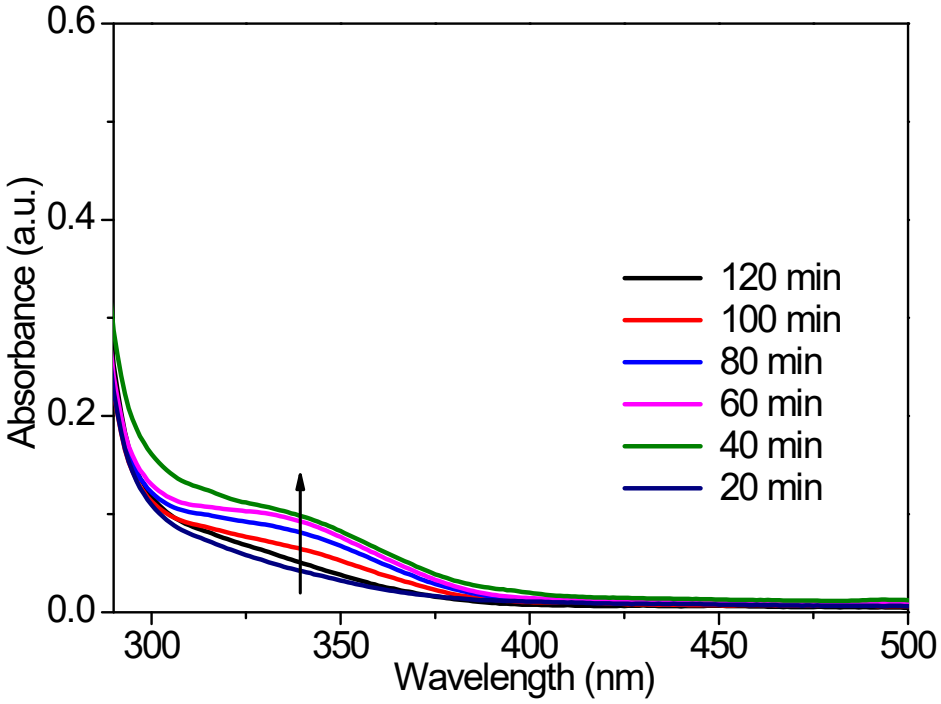

Figure S23. UV−vis spectra of the NADH regeneration reaction solution with Rh1/SCA/p-Si as a catalyst.

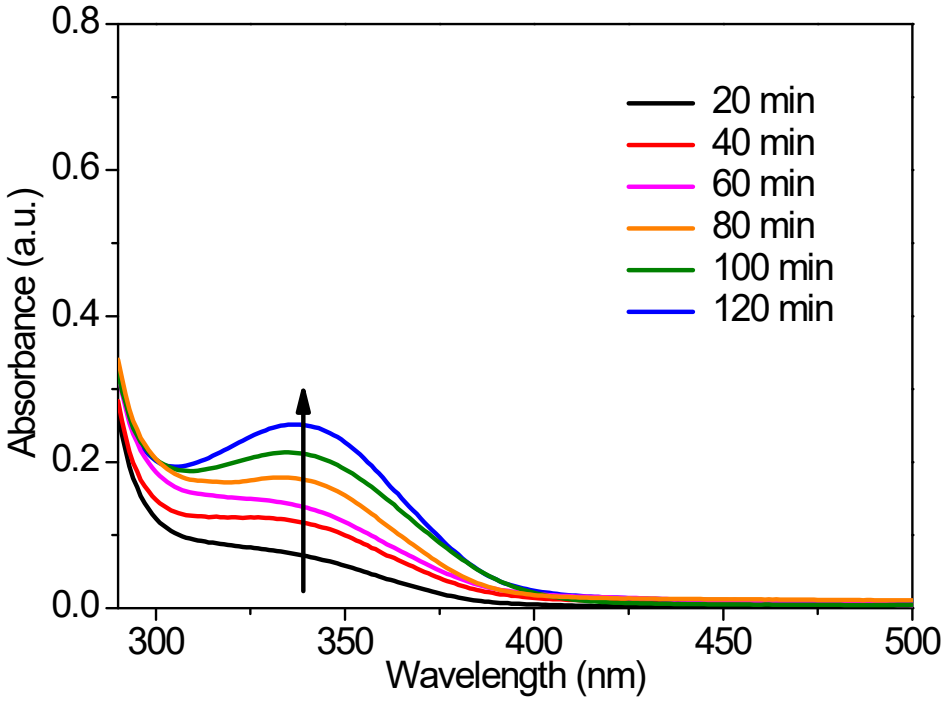

Figure S24. UV−vis spectra of the NADH regeneration reaction solution with Rh1/OBV^{2+}/SCA/p-Si as a catalyst.

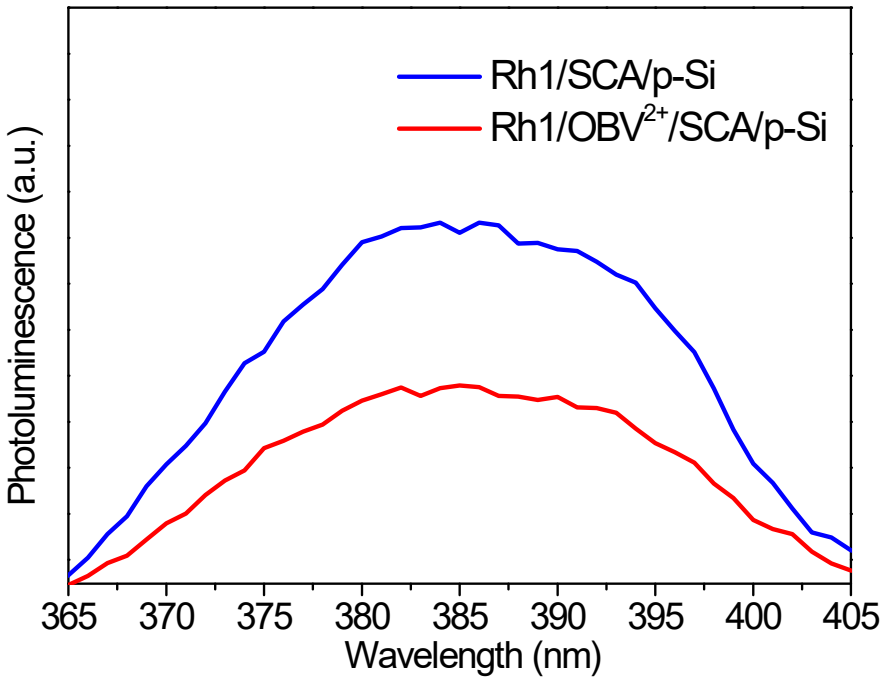

Figure S25. Steady-state photoluminescence spectra at 385 nm of Rh1/OBV^{2+}/SCA/p-Si and Rh1/SCA/p-Si photocathodes.

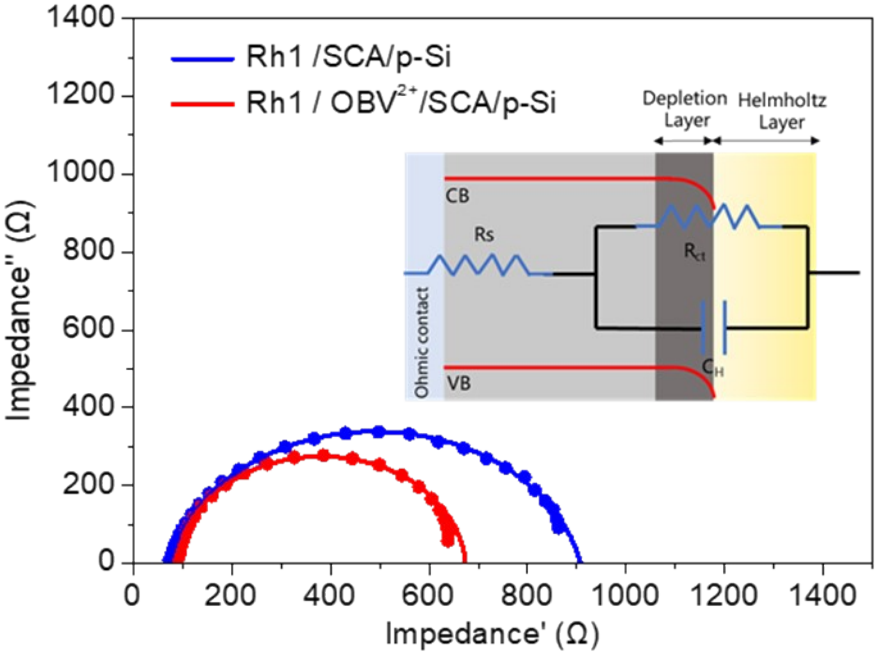

Figure S26. Nyquist plots from PEIS experiments, fitting curves shown by solid lines, and the inset is the equivalent circuit.

	Rh1/OBV2+/SCA/p-Si	Rh1/SCA/p-Si
Rs(Ω)	88.9	72.1
R_{ct}(Ω)	590	835
C_H(μF)	0.394	0.738
Error(%)	4.87	3.94

Table S1. values of resistances and capacitances

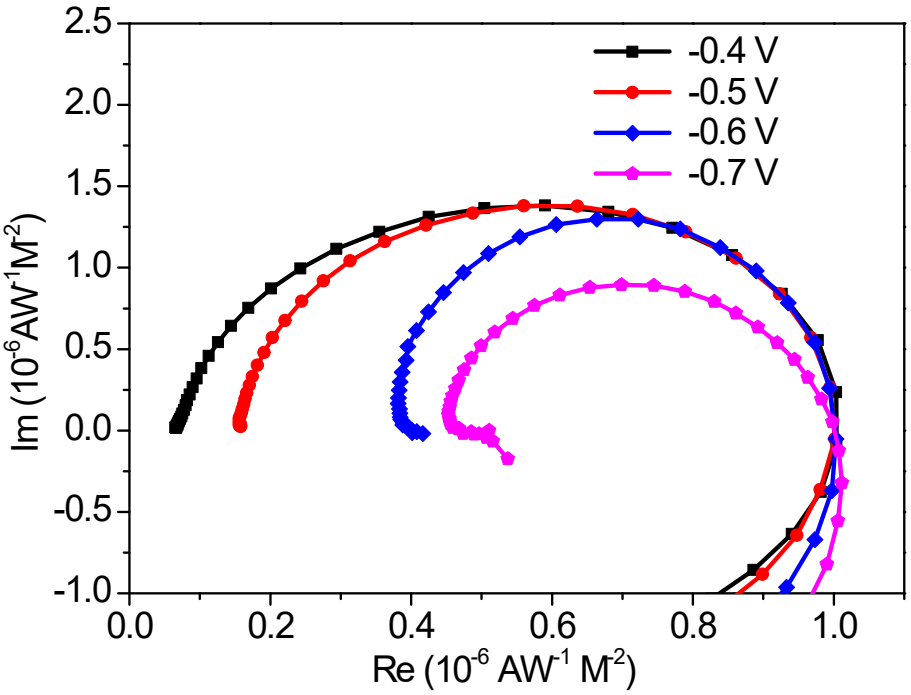

Figure *S27.* IMPS curves of Rh1/OBV^{2+}/SCA/p-Si measured at different potentials.

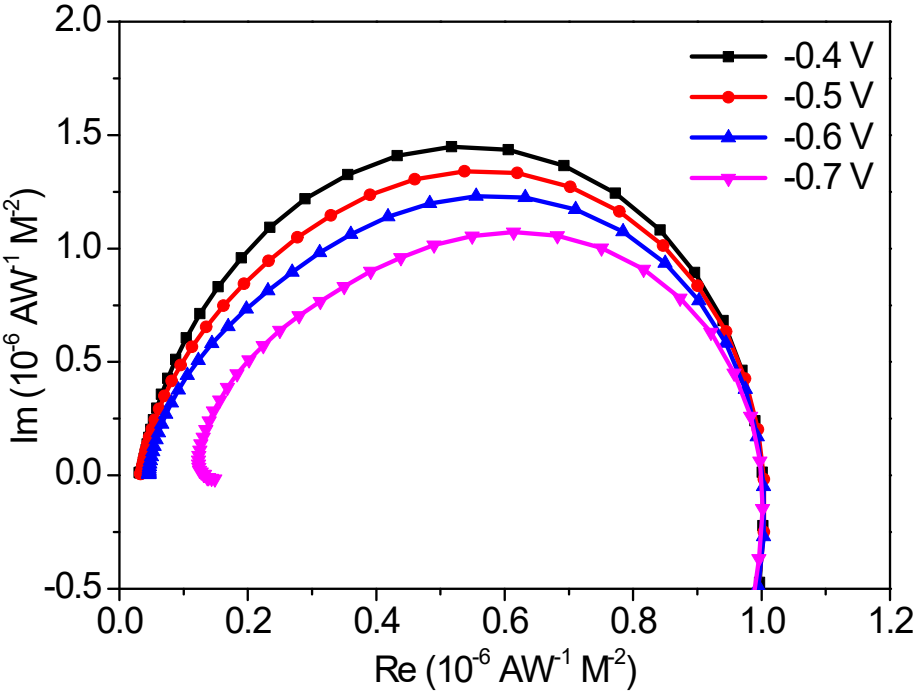

Figure *S28.* IMPS curves of Rh1/SCA/p-Si measured at different potentials.

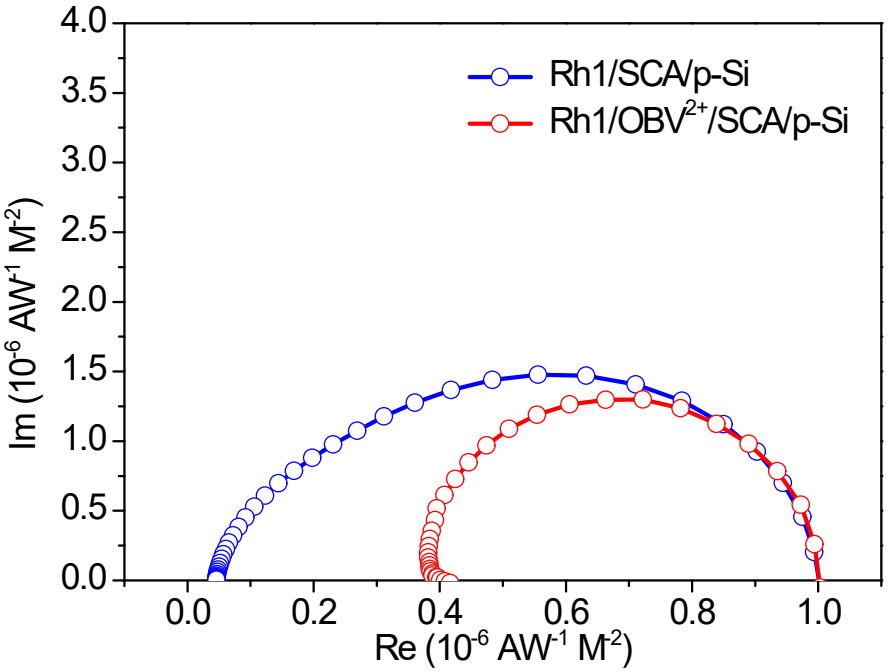

Figure S29. IMPS spectra of photocathodes at −0.6 V vs. RHE.

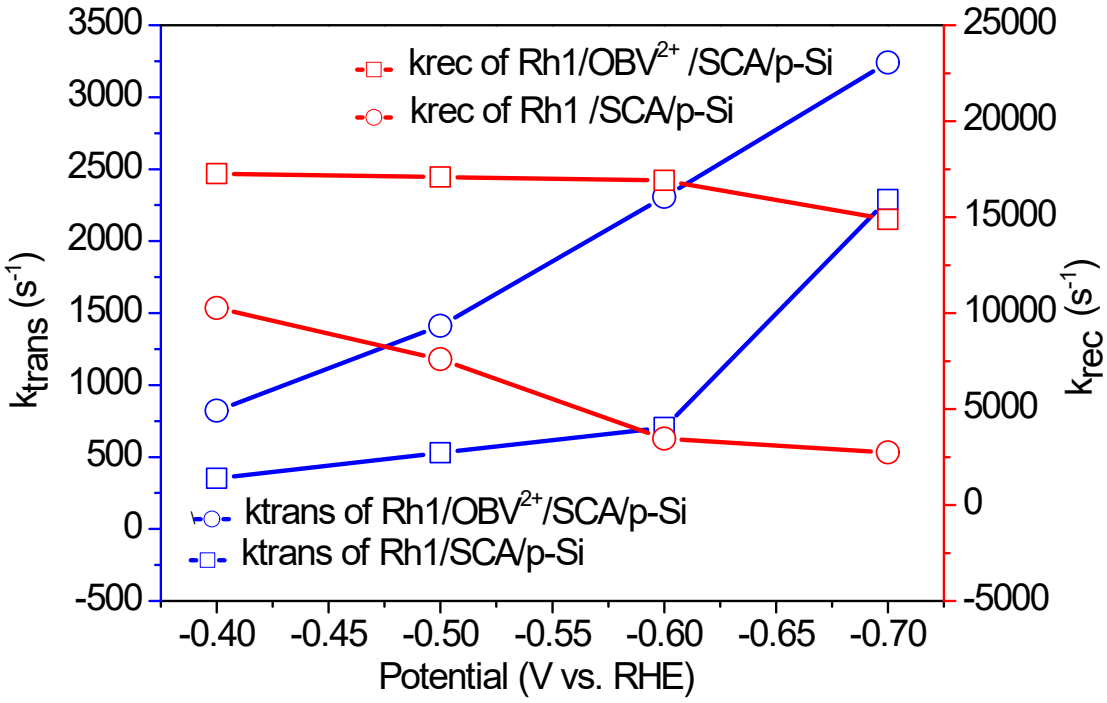

Figure S30. Rate constants of charge recombination (k_{rec}) and charge transfer (k_{trans}) at different potentials.